Divalent Cations and Lipid Composition Modulate Membrane Insertion and Cancer-Targeting Action of pHLIP

Victor Vasquez-Montes [1], Janessa Gerhart [2], Damien Thévenin [2] and Alexey S. Ladokhin [1]

1 - Department of Biochemistry and Molecular Biology, *The University of Kansas Medical Center, Kansas City, KS, 66160, USA*
2 - Department of Chemistry, *Lehigh University, 6 East Packer Avenue, Bethlehem, PA, 18015, USA*

Correspondence to Alexey S. Ladokhin: *Fax: +913 588-7440. aladokhin@kumc.edu*
https://doi.org/10.1016/j.jmb.2019.10.016
Edited by P. Wright

Abstract

The pH-Low Insertion Peptide (pHLIP) has emerged as an important tool for targeting cancer cells; it has been assumed that its targeting mechanism depends solely on the mild acidic environment surrounding tumors. Here, we examine the role of Ca^{2+} and Mg^{2+} on pHLIP's insertion, cellular targeting, and drug delivery. We demonstrate that physiologically relevant concentrations of either cation can shift the protonation-dependent transition by up to several pH units toward basic pH and induce substantial protonation-independent transmembrane insertion of pHLIP at pH as high as 10. Consistent with these results, the ability of pHLIP to deliver the cytotoxic compound monomethyl-auristatin-F to HeLa cells is increased several fold in presence of Ca^{2+}. Complementary measurements with model membranes confirmed this Ca^{2+}/Mg^{2+}-dependent membrane-insertion mechanism. The magnitude of this alternative Ca^{2+}/Mg^{2+}-dependent effect is also modulated by lipid composition—specifically by the presence of phosphatidylserine—providing new clues to pHLIP's unique tumor-targeting ability in vivo. These results exemplify the complex coupling between protonation of anionic residues and lipid-selective targeting by divalent cations, which is relevant to the general signaling on membrane interfaces.

Introduction

The selective targeting of tumors is an important aspect of developing and optimizing anticancer therapies. In the past decade, the pH-Low Insertion Peptide (pHLIP) has emerged as a promising tool in tumor imaging and targeted drug delivery [1–5]. pHLIP remains stable in solution, yet it can also insert into membranes under mildly acidic (pH ~ 6) conditions and translocate cargo molecules (including anticancer drugs) conjugated to its C-terminus across the lipid bilayer [5–8]. Model *in vitro* studies suggest that the interaction of pHLIP with lipid membranes involves an initial interfacial binding of unfolded peptide at neutral pH, with subsequent insertion as a transmembrane helix upon acidification [9,10]. The latter is believed to be the molecular mechanism responsible for pHLIP's selective targeting of tumors, which are known to produce a slightly more acidic extracellular microenvironment (pH ~ 7) than healthy tissues (pH 7.4) [11,12]. The advent of pHLIP has led to the development of other promising protonation-driven cancer targeting peptides like ATRAM [13] and TYPE7 [14], with a supposedly similar mode of action. Whether such a small difference in pH can solely explain the selectivity of pHLIP toward tumors in vivo, or whether other mechanisms are involved remains unknown.

One of the biggest challenges in deciphering the molecular mechanisms driving pHLIP tumor targeting arises from the often-overlooked discrepancy in experimental conditions between the studies aimed at delivering compounds into cancer cells and studies with model lipid vesicles. While delivery studies into cells are normally performed in the presence of physiological concentrations of divalent ions (present in growth media or extracellular fluid) [6,15,16], experiments with vesicles have been, so far, conducted in the absence of Ca^{2+} or Mg^{2+} [10,17–21]. Furthermore, most mechanistic studies

have been performed on vesicles containing only phosphatidylcholine, thus neglecting the complex nature of the plasma membrane. For instance, we have previously demonstrated that variation in lipid composition leads to a significant variation in the apparent pK_a of the insertion of pHLIP [19,20]. Here, we examine the role of lipid composition and divalent cations in the pHLIP targeting of both model membranes and cancer cells. Using a combination of spectroscopic and cellular techniques, we show that the membrane insertion of pHLIP is strongly promoted by physiological concentrations of Ca^{2+} and Mg^{2+}. Our results also suggest a strong regulatory link between membrane lipid composition and extracellular concentrations of Ca^{2+}/Mg^{2+} on the membrane insertion of pHLIP, which may have general implications for signaling on membrane interfaces.

Results

Ca^2 promotes the cellular interaction of pHLIP

The cellular interaction between pHLIP, labeled at its N-terminus with the fluorophore Alexa488 (A488-pHLIP), and human MDA-MB-231 breast cancer cells was inspected by fluorescence microscopy under two different conditions: (1) in the absence of divalent cations to reflect conditions most commonly used to characterize pHLIP interactions with vesicles and (2) in the presence of 1.8 mM Ca^{2+}, as a simplified mimetic of extracellular divalent cation concentration. In both cases, cells are incubated with A488-pHLIP at the appropriate pH, washed, and imaged. No significant fluorescence was observed at pH 7.4 in the absence of divalent cations (Fig. 1b), pointing to a weak cellular interaction of pHLIP-A488 under these conditions. It should be noted that the formation of the interfacial form of the peptide is still expected, but likely removed by the washes performed before microscopy imaging. As expected, acidification of the solution to pH 6.0 resulted in a large increase in A488 fluorescence intensity (Fig. 1a), attributed to the pH-dependent membrane insertion character of pHLIP. At a pH of 7.4, the addition of 1.8 mM Ca^{2+} also resulted in a significant increase in A488 fluorescence intensity (Fig. 1c), suggesting that the presence of Ca^{2+} induces the interaction of A488-pHLIP with cellular membranes without the need for acidification.

The effect of Ca^{2+} on pHLIP cellular interactions was quantified by flow cytometry. At pH 7.4, the presence of Ca^{2+} led to a concentration-dependent increase in A488 fluorescence, with a 1.8- and 2.8-fold increase at 1.2 and 1.8 mM Ca^{2+}, respectively (Fig. 1g). These results are consistent with the fluorescence increase observed by microscopy (Fig. 1a–f) and confirm the ability of Ca^{2+} to promote

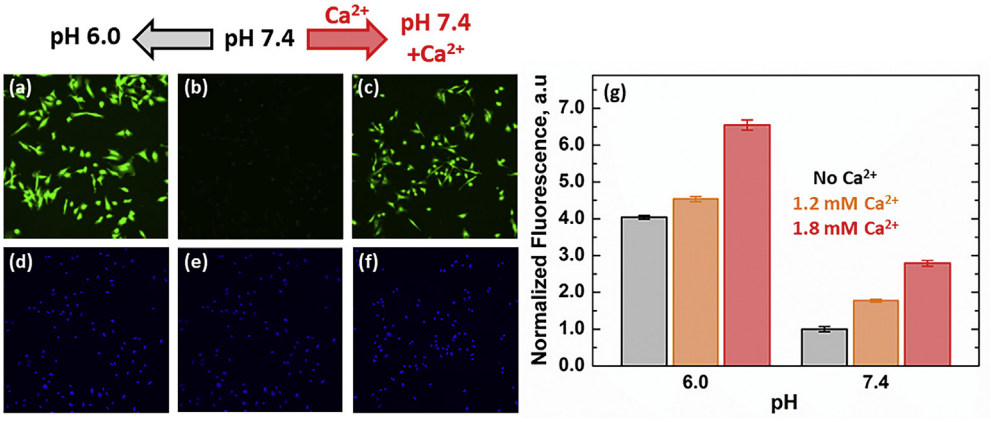

Fig. 1. Comparison of pH-dependent and Ca^2-dependent cellular targeting by pH-Low Insertion Peptide (pHLIP). The cellular interaction of pHLIP N-terminally conjugated to an Alexa488 fluorophore (A488-pHLIP) was determined by fluorescence microscopy (a–f) and flow cytometry (g) using MDA-MB-231 cells. (a–c) An increase in A488 intensity (green), indicative of pHLIP cellular interaction, was observed either by acidification (a) or the addition of 1.8 mM Ca^{2+} at pH 7.4 (c) to a sample at pH 7.4 lacking Ca^{2+} (b). (d, f) Hoechst staining of MDA-MB-231 cells used in microscopy images. (g) Flow cytometry was used to quantify the effects of $[Ca^{2+}]$ on the interaction of A488-pHLIP with MDA-MB-231 cells at pH 7.4 to mimic the extracellular pH of healthy cells or at mildly acidic pH 6.0. At both pH the presence of Ca^{2+} led to higher fluorescence, due to larger populations of membrane bound pHLIP. Normalized fluorescence represents the fold increase over cells incubated without Ca^{2+} at pH 7.4. Data are represented as mean values from which the error bars represent the standard error of the mean ($n = 3$). Representative microscopy images of conditions used in flow cytometry measurements are shown in Fig. S1.

the interaction of pHLIP with cells. A similar trend was observed when cells were incubated with A488-pHLIP at pH 6.0, albeit with higher A488 intensity, likely due to the pH-dependent insertion of pHLIP. Representative microscopy images of the conditions used in the flow cytometry measurements are shown in Fig. S1. These results indicate that acidic conditions and Ca^{2+} work in tandem to induce the interaction of pHLIP with cells and its possible membrane insertion. Understanding the role of divalent cations as possible regulators of pHLIP membrane interaction is, therefore, critical to establishing the molecular mechanism of pHLIP under physiological conditions.

Ca^2 promotes pHLIP-mediated translocation of cargo molecules and cytotoxicity

We evaluated the effect that Ca^{2+} may have on the ability of membrane-inserted pHLIP to translocate cargo molecules into cancer cells using a construct, in which the cytotoxic agent MMAF (monomethyl auristatin F) is conjugated to the C-terminus of pHLIP via a disulfide bond (pHLIP-MMAF). We know from our previous reports that pHLIP can translocate, release MMAF into the cytoplasm, and induce cancer cell death in a pH-dependent manner [22,23]. The presence of 1.2 mM Ca^{2+} greatly increased cytotoxicity at pH 7.4, indicated by an at least 10-fold decrease in the IC_{50} from $\geq$8.5 μM in the absence of Ca^{2+} (Fig. 2a, black) to 0.9 ± 0.1 μM (Fig. 2a, red). The decrease in cellular viability observed in absence of Ca^{2+} is attributed to nonspecific killing due to background levels of endocytosis upon association of pHLIP-MMAF to cell membranes, as we previously reported [22,23]. Nevertheless, these results are consistent with the increase in A488 intensity observed by microscopy and flow cytometry (Fig. 1) and indicates that Ca^{2+} promotes the interaction of pHLIP with cells, and possibly its transmembrane insertion.

Treating cells with pHLIP-MMAF at pH 6.0 in the absence Ca^{2+} led to a 5-fold decrease in IC_{50} (1.6 ± 0.1 μM; Fig. 2b, black) as compared with pH 7.4 ($\geq$8.5 μM; Fig. 2a, black). Inclusion of Ca^{2+} in the treatment solution resulted in another 5-fold decrease in IC_{50} (0.3 ± 0.1 μM; Fig. 2b, red). The addition of Ca^{2+} not only resulted in lower IC_{50} values, but also in a steeper cytotoxicity response. We attribute this change to a more favorable transmembrane insertion of pHLIP and subsequent drug delivery in the presence of Ca^{2+}. The increased cooperativity led to a 10-fold difference in the concentration of pHLIP-MMAF required to kill 80% of cells between both conditions tested. Where 0.53 μM pHLIP-MMAF was sufficient to kill 80% of cells at pH 6.0 in the presence of Ca^{2+}, while an equimolar concentration of pHLIP-MMAF only resulted in 23% cytotoxicity in the absence of Ca^{2+}.

Our cytotoxicity results, together with the fluorescence microscopy (Fig. 1a–c) and flow cytometry measurements (Fig. 1g), show that the presence of physiological Ca^{2+} concentrations promote the ability of pHLIP to translocate compounds across cellular membranes. Physiological conditions must therefore be considered when characterizing and

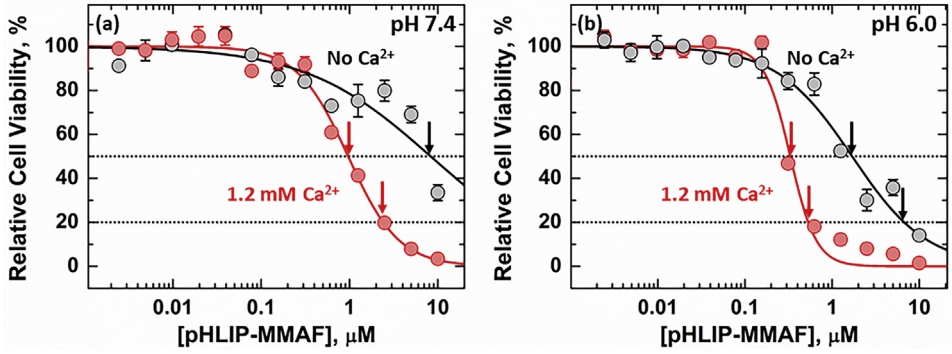

Fig. 2. Effect of pHLIP-MMAF treatment on the viability of cultured of HeLa cells. The directional insertion of pH-Low Insertion Peptide (pHLIP) results in the intracellular delivery of C-terminally conjugated monomethyl auristatin F (MMAF), which is then released into the cytosol through cleavage of the connecting disulfide bond by the reducing cytosolic environment. Measurements were performed at pH 7.4 and 6.0 in the presence or absence of 1.2 mM Ca^{2+} (the extracellular [Ca^{2+}] at pH 7.4). At both pH 7.4 and 6.0, the presence of Ca^{2+} led to higher cytotoxicity likely due to the more favorable insertion of pHLIP into cell membranes, and the subsequent increased translocation of MMAF into cells. Horizontal dotted lines and color-coded arrows indicate the concentration of pHLIP-MMAF required to kill 50% and 80% cells under each condition tested. (a) At pH 7.4, the presence of Ca^{2+} at pH 7.4 resulted in a 10-fold decrease of the IC_{50} from $\geq$8.5 to 0.9 ± 0.1 μM. (b) At pH 6.0, addition of Ca^{2+} led to a 5-fold decrease in IC_{50} from 1.6 ± 0.1 to 0.3 ± 0.1 μM. The increased steepness of the transition led to a 10-fold difference in the [pHLIP-MMMAF] required to kill 80% of cells. All measurements were normalized to the media control (0 μM, pH 7.4), as 100% cell viability, in which the error bars represent standard error of the mean (n = 3).

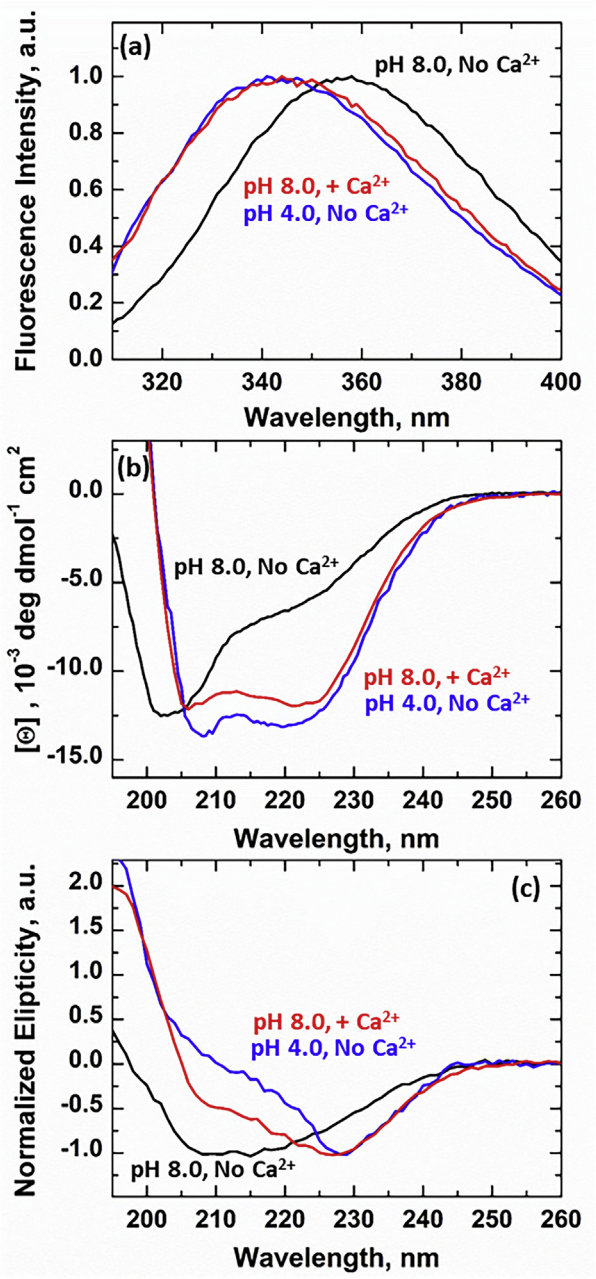

Fig. 3. Comparison of pH-dependent and Ca^{2}-dependent insertion of pH-Low Insertion Peptide (pHLIP) into model palmitoyl-oleoyl-phosphatidylcholine(POPC) membranes. The transmembrane insertion of pHLIP was characterized by (a) Trp fluorescence and (b) circular dichroism (CD) in large unilamellar vesicles (LUV) and by oriented circular dichroism (OCD) in flat multilayers. (a) At pH 8.0, the interfacial form pHLIP presents a Trp position of maximum of 354 nm (black). Acidification of the sample to pH 4.0 leads to a 12 nm blue shift to 342 nm, characteristic of pHLIP's transmembrane State III (blue) [10]. Introducing 2.0 mM Ca^{2+} (a proxy for extracellular divalent cation concentration) while maintaining the pH constant at 8.0 results in a similar 9 nm blue shift to 345 nm (red). (b) CD measurements in the absence of Ca^{2+} at pH 8.0 (black) and 4.0 (blue) show characteristic signals for unstructured peptides and α-helices, respectively, consistent with its previously reported pH-dependent transmembrane insertion [10]. The addition of 1.0 mM Ca^{2+} at pH 8.0 resulted in a typical α-helical spectrum (red) with a similar ellipticity as the one observed at pH 4.0 in the absence of Ca^{2+}. (c) OCD measurements were performed in the presence of Ca^{2+} at pH 8.0 (red); and in the absence of Ca^{2+} at pH 4.0 (blue) and 8.0 (black). The latter two conditions correspond to those of the transmembrane State III and interfacial State II of pHLIP, respectively. The Ca^{2+}-inserted and pH-inserted samples exhibited similar spectra with a single minimum ~228 nm, characteristic of the OCD spectra of transmembrane α-helices [25].

optimizing the interaction and mechanism of pHLIP-like cancer targeting systems.

Ca^{2}-dependent transmembrane insertion into model POPC membranes

The common way of characterizing pH-dependent membrane interactions of pHLIP is through a combination of changes in its tryptophan (Trp) emission maximum and circular dichroism (CD) spectrum [10,17–21]. Here, we used these techniques to compare the spectral responses of pHLIP observed at neutral pH in the presence of Ca^{2+} with those observed on transmembrane insertion at acidic pH.

The spectral hallmarks of the interfacial (State II) and transmembrane (State III) states of pHLIP have been firmly established by previous studies [10,19,24]. Our data collected in the absence of Ca^{2+} are consistent with these hallmarks (Fig. 3). Specifically, the Trp fluorescence maximum of the interfacial State II of pHLIP (populated in the presence of large unilamellar vesicles [LUV] composed of palmitoyl-oleoyl-phosphatidylcholine [POPC] at pH 8.0) is 354 nm (Fig. 3a, black), indicating that the Trps are in a relatively polar environment. In State III (populated at pH 4), the maximum is blue-shifted to 342 nm (Fig. 3a, blue), consistent with a more nonpolar environment. Our data collected at pH 8, but in the presence of 2.0 mM Ca^{2+} (Fig. 3a, red), clearly indicate that, under these conditions, pHLIP exhibits fluorescence hallmarks of the transmembrane State III.

A similar pattern is observed with conformational changes measured by CD spectroscopy for solution samples containing LUV (Fig. 3b) or samples in oriented multilayers (Fig. 3c). In the absence of Ca^{2+} at pH 8.0, the CD spectrum of pHLIP showed a single minimum ~200 nm, typical of unstructured peptides and consistent with the largely unfolded interfacial State II (Fig. 3b, black) [10]. In contrast, the CD spectra of pHLIP collected at pH 4.0 in the

absence of Ca^{2+} (transmembrane State III) and at pH 8.0 in the presence of Ca^{2+} were equivalent (Fig. 3b, blue and red), with both spectra presenting a double minimum at ~208 and 222 nm, characteristic of α-helices.

The pH- and Ca^{2+}-induced helices also have similar orientations with respect to membrane normal, as revealed by the oriented circular dichroism (OCD) measurements performed in lipid multilayers (Fig. 3c). Both OCD spectra (red and blue curves) have a single sharp minimum at 228 nm, characteristic of transmembrane α-helices [25,28,29]. The spectra are also consistent with the previously reported OCD spectrum of the transmembrane State III of pHLIP [26,27]. As expected, these spectra are quite different from that measured at pH 8.0 in the absence of Ca^{2+} (black line), *i.e.,* under conditions corresponding to the interfacial State II. Together, all fluorescence and CD measurements indicate that the Ca^{2+}-inserted state resides in the lipid bilayer in the same conformation as the conventional pH-inserted transmembrane State III of pHLIP.

Effects of lipid composition on the Ca^2-mediated insertion of pHLIP

One of the hallmarks of cancer cells is the change in lipid composition of the outer leaflet of the plasma membrane, specifically the increase in phosphatidylethanolamine (PE) and phosphatidylserine (PS) [28–32]. Previously, we have established that additions of many non-PC lipids, including PE and PS, have a substantial effect on the pH-dependent insertion of pHLIP [19,20]. Here, we compared how the membrane insertion of pHLIP into pure POPC bilayers and bilayers containing 25% of either 1-palmitoyol-2-oleoyl-*sn-glycero-3-phosphoethanolamine (*POPE) or palmitoyl-oleoyl-phosphatidylserine (POPS) is affected by the presence of Ca^{2+}.

Trp emission spectra were collected in the presence of POPC LUV at pH 10.0 and increasing Ca^{2+} concentrations to characterize the Ca^{2+}-mediated membrane insertion of pHLIP. The positions of their maxima were then compared with the known maxima of the interfacial State II (Fig. 4a red dashed line) and transmembrane State III (Fig. 4a blue dashed line) forms of pHLIP at pH 10.0 and 4.0, respectively. Incremental addition of Ca^{2+} at pH 10.0 led to progressive decreases in pHLIP Trp maxima until they approached saturation at 343 nm in 5.0 mM Ca^{2+} (Fig. 4a, filled circles). The positions of maxima observed at 4.0–5.0 mM Ca^{2+} match those observed for the transmembrane State III of pHLIP. Together with the α-helical conformation determined by CD (Fig. 3b) and transmembrane orientation determined by OCD (Fig. 3c), these results confirm that Ca^{2+} induces the transition of pHLIP into its transmembrane State III. These results also imply that 2.0 mM Ca^{2+}, a proxy for extracellular divalent cation concentration, is sufficient to induce the transmembrane insertion of ~70% of pHLIP present in the sample at pH 10.0. The Ca^{2+}-dependent blue shifts were reversible in the presence of EDTA (Fig. 4a, open circles).

Control measurements in the absence of membranes were performed to confirm that the Ca^{2+}-dependent Trp blue shifts were not caused by aggregation-induced Trp burial. No significant changes in the Trp emission spectrum of pHLIP were observed after the addition of Ca^{2+} (356 nm, Fig. S2a, red) as compared with samples lacking Ca^{2+} (357 nm, Fig. S2b, black). This indicates that the results observed in the presence of LUV are membrane-dependent and not due to peptide aggregation. The small 1 nm blue shift from 357 nm after the addition of Ca^{2+} suggests, however, that Ca^{2+} likely affects the unstructured "conformation" of pHLIP in solution. Moreover, the effect of Ca^{2+} concentration on the aggregation of POPC LUV was also tested by light scattering measurements. No Ca^{2+}-dependent membrane aggregation of POPC LUV was detected under the concentrations used in this study (Fig. S3a).

We next characterized the effect of Ca^{2+} on the protonation-dependent insertion of pHLIP into POPC LUV using intrinsic Trp fluorescence as a function of pH. In the absence of Ca^{2+}, the pH-dependent insertion of pHLIP into POPC bilayers yielded a protonation-dependent membrane insertion pK_a of 6.1 ± 0.1 (Fig. 4b, black), consistent with previous reports [21,33]. The presence of 2.0 mM Ca^{2+} (Fig. 4b, brown) led to two prominent changes in the pH-dependent insertion of pHLIP: (1) A pronounced decrease in the Trp fluorescence maximum at pH 10.0 (Fig. 4b, red arrow) and (2) a significant shift of the titration curve toward basic pH (Fig. 4b, blue arrow). The 7 nm blue shift at pH 10.0 from 354 nm to 347 likely reflects the Ca^{2+}-mediated membrane insertion of pHLIP independent of pH. The presence of 2.0 mM Ca^{2+} also led to a 1.5 pH-unit shift in the pK_a of the titration curve to 7.6 ± 0.1 (Fig. 4b, brown) compared with 6.1 ± 0.1 in the absence of Ca^{2+} (Fig. 4b, black). These results, together with our measurements at constant pH 10.0 (Fig. 4a), indicate a dual effect for Ca^{2+} on the interaction of pHLIP with POPC membranes: (1) Ca^{2+} induces the transmembrane insertion of a significant fraction of the pHLIP population without need of acidification. (2) Ca^{2+} promotes the pH-dependent transmembrane insertion of the remaining interfacial population.

Measurements were replicated with LUV containing 25% of the zwitterionic lipid POPE or the anionic lipid POPS. The addition of POPE or POPS-containing LUV did not result in the characteristic 4 nm Trp blue shift associated with the interfacial State II of pHLIP in the absence of Ca^{2+}. This effect has been

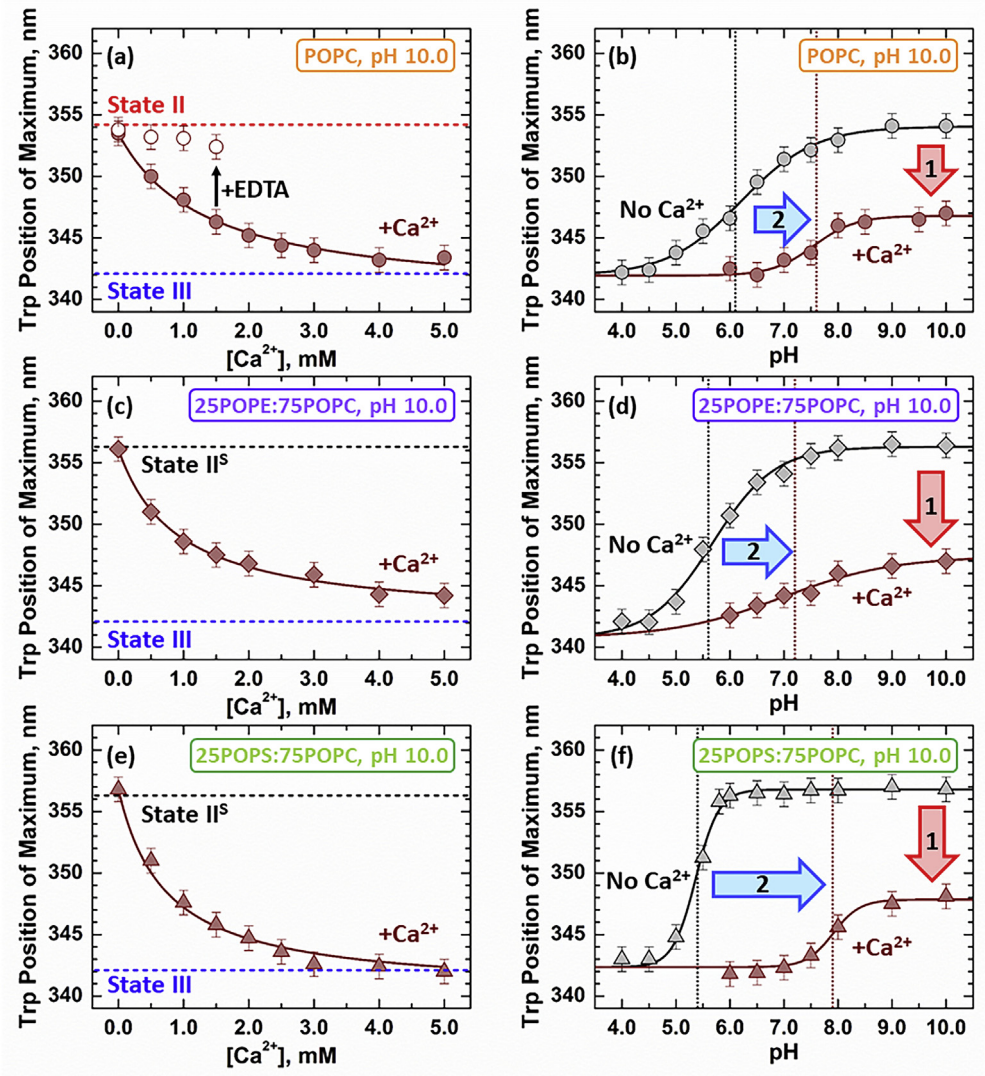

Fig. 4. Lipid modulation of Ca^2-dependent membrane interactions of pH-Low Insertion Peptide (pHLIP). Ca^{2+} titrations at constant pH 10.0 and pH-titrations in the presence of 2.0 mM Ca^{2+} were performed in the presence of POPC (a, b), 25POPE:75POPC (c, d), or 25POPS:75POPC (e, f) large unilamellar vesicles (LUV). (a, c, and e) The intrinsic fluorescence of pHLIP was measured at pH 10.0 and increasing [Ca^{2+}]. Positions maximum for the two known interfacial forms of pHLIP (State II in POPC and II^S in non-POPC LUV) and transmembrane State III are indicated by the horizontal dashed lines [20]. Incremental addition of Ca^{2+} at pH 10.0 resulted in large concentration dependent blue shifts regardless of lipid composition (filled circles). In all cases, saturation was achieved at the Trp positions of maxima expected for the transmembrane State III of pHLIP. The large spectral changes observed show that Ca^{2+} induces the transmembrane insertion of pHLIP without any acidification, even at pH 10.0 (red arrows). Addition of EDTA reversed the Ca^{2+}-dependent spectral changes (open circles). (b, d, and f) The presence of 2.0 mM Ca^{2+} promoted the pH-dependent insertion of pHLIP into all LUV compositions tested, indicated as an increase in its transition pK_a (blue arrows). A 1.5 pH unit increase was observed in POPC from 6.1 ± 0.1 to 7.6 ± 0.1 and in 25POPE:75POPC from 5.7 ± 0.1 to 7.2 ± 0.1. While a larger 2.4 pH unit shift from 5.4 ± 0.1 to 7.8 ± 0.1 was detected in 25POPS:75POPC LUV. The transition pK_a of each curve is graphically indicated by color-coded vertical dotted lines. POPC, palmitoyl-oleoyl-phosphatidylcholine; POPE, 1-palmitoyol-2-oleoyl-*sn-glycero-3-phosphoethanolamine; POPS, palmitoyl-oleoyl-phosphatidylserine.*

previously described and relates to the formation of the spectroscopically silent interfacial State II^S (Fig. 4c and e, black dashed line) [20]. Regardless of the starting interfacial form, the incremental addition of Ca^{2+} resulted in concentration-dependent Trp blue shifts. The observed endpoint between the different LUV used were similar with a 12 nm decrease from 356 nm in the absence of Ca^{2+} to 344 nm at 5.0 mM Ca^{2+} observed for 25POPE:75-POPC (Fig. 4c). While a 14 nm decrease from

356 nm to 342 nm was observed in the case of 25POPS:75POPC LUV under the same conditions (Fig. 4e). Compared with zwitterionic POPC and POPE membranes, the Ca^{2+}-dependent transition of pHLIP into its transmembrane State III was significantly steeper in the presence of the anionic POPS lipids. This suggests that the POPS lipids exposed in the membranes of cancer cells promote the Ca^{2+}-dependent membrane insertion of pHLIP.

The pH-dependent insertion of pHLIP was also measured for 25POPE:75POPC (Fig. 4c and d) and 25POPS:75POPC LUV (Fig. 4e and f). Overall the effects of Ca^{2+} in these lipid compositions are qualitatively similar to those in pure POPC (Fig. 4a and b) and are characterized by the induction of insertion at neutral and basic pH (arrow 1, Fig. 4b, d and f) and changes in pK_a for acid-induced insertion (arrow 2). The quantitative effects, however, are lipid dependent. In the absence of Ca^{2+}, the lipid-dependent changes in pK_a are consistent with those reported previously [17,19,20]. Namely, the insertion in mixed lipid compositions requires stronger acidic environment (e.g., $pK_a = 5.7 \pm 0.1$ in 25POPE:75POPC LUV and a $pK_a = 5.4 \pm 0.1$ in 25POPS:75POPC LUV) as compared to pure POPC ($pK_a = 6.1 \pm 0.1$ for POPC). The presence of 2.0 mM Ca^{2+} leads to a blue shift in the Trp fluorescence maxima at pH 10.0 as well as a move of the titration curves toward alkali pH, regardless of lipid composition. The magnitude of the associated changes, however, is modulated by lipid composition and was particularly prominent for the protonation-dependent insertion of pHLIP. In the case of the zwitterionic 25POPE:75POPC LUV, the presence of Ca^{2+} led to a 1.5 pH unit increase in pK_a from 5.7 to 7.2 (Fig. 4d). Meanwhile, the anionic 25POPS:75POPC LUV showed a larger 2.4 pH unit increase from 5.4 to 7.8 between samples lacking and containing Ca^{2+}, respectively (Fig. 4d). Together with the Ca^{2+} titration measurements, these results reveal a strong lipid dependence for the Ca^{2+}-dependent modulation of pHLIP membrane insertion with a strong preference toward anionic POPS bilayers.

Effects of Ca^2 on the thermodynamics of pHLIP membrane insertion

Our measurements of pHLIP insertion in the presence of Ca^{2+} demonstrated the simultaneous presence of two distinct effects: (1) induction of protonation-independent membrane insertion at neutral and basic pH (Fig. 4a, c, and e) and (2) shift of the protonation-dependent insertion toward more neutral pHs (Fig. 4b, d, and f). To quantify the thermodynamics of both processes, we repeated the same experiments done at 2.0 mM Ca^{2+} (presented in Fig. 4) at intermediate [Ca^{2+}] (Fig. S4).

The thermodynamics of the protonation-independent membrane insertion of pHLIP was characterized with the free energy term $\Delta G_{TM}^{[Ca2+]}$. This term was derived from the fractional insertion, f_{TM}, which was calculated using the changes in fluorescence emission maximum (Eq. (4)) at pH 10.0 for each [Ca^{2+}] tested in our pH-titrations (Fig. S4). This thermodynamic approach is essentially identical to that used in the derivation of the so-called biological hydrophobicity scale [34] and in the quantitation of insertion by molecular dynamics simulations [35]. The results presented in Fig. 5a demonstrate that all lipid compositions present a similar susceptibility to this process, particularly at [Ca^{2+}] $\geq$ 1.0 mM. At lower [Ca^{2+}], however, membranes composed purely of POPC lipids show a lower susceptibility than the mixed lipid compositions. Nevertheless, at least half of the population of pHLIP is already inserted at the physiologically relevant concentrations of extracellular Ca^{2+}at neutral and basic pH.

To examine the effects of Ca^{2+} on the thermodynamics of protonation-dependent insertion, we used the same procedure employed in our previous publications on the lipid-dependent modulation of pHLIP insertion [19,20]. Specifically, we used pH-titration plots to determine the apparent pK_a for the insertion transition (Eq. (2)), from which the free energy was calculated using Eq. (3). The results presented in Fig. 5b show that the effect in pure POPC and 25POPE:75POPC mixtures is almost indistinguishable and saturates at about 2 kcal/mol after 1.0 mM Ca^{2+} is present. In contrast, the gain in free energy of protonation-dependent insertion in 25POPS:75POPC is more pronounced and reaches 3.0 kcal/mol at 2.0 mM Ca^{2+}. Interesting observations come from a cross-correlation analysis, in which the protonation-dependent gain in free energy is plotted against the protonation-independent (calcium-induced) free energy of insertion (Fig. 5c). Remarkably, the correlations are linear, yet the slope varies dramatically with lipid composition, suggesting that the lipid composition modulates the interplay of various modes of pHLIP membrane insertion on a thermodynamic level (see Discussion).

Comparison of Ca^2 and Mg^2-dependent effects

To determine whether other divalent cations exhibited an effect similar to that of Ca^{2+}, we repeated our experiments with LUV in the presence of 2.0 mM Mg^{2+}. Similar to Ca^{2+}, incremental increases in [Mg^{2+}] at constant pH 10.0 in the presence of POPC LUV showed concentration-dependent Trp blue shifts (Fig. S5a). The end point at saturating Mg^{2+} concentrations, however, did not reach the expected Trp fluorescence maximum for the transmembrane State III. Instead, the signal saturated at ~348 nm, 6 nm higher than the 342 nm expected when the entire population is present in its transmembrane conformation (Fig. 4a). Similarly, Mg^{2+} titrations in the presence of zwitterionic

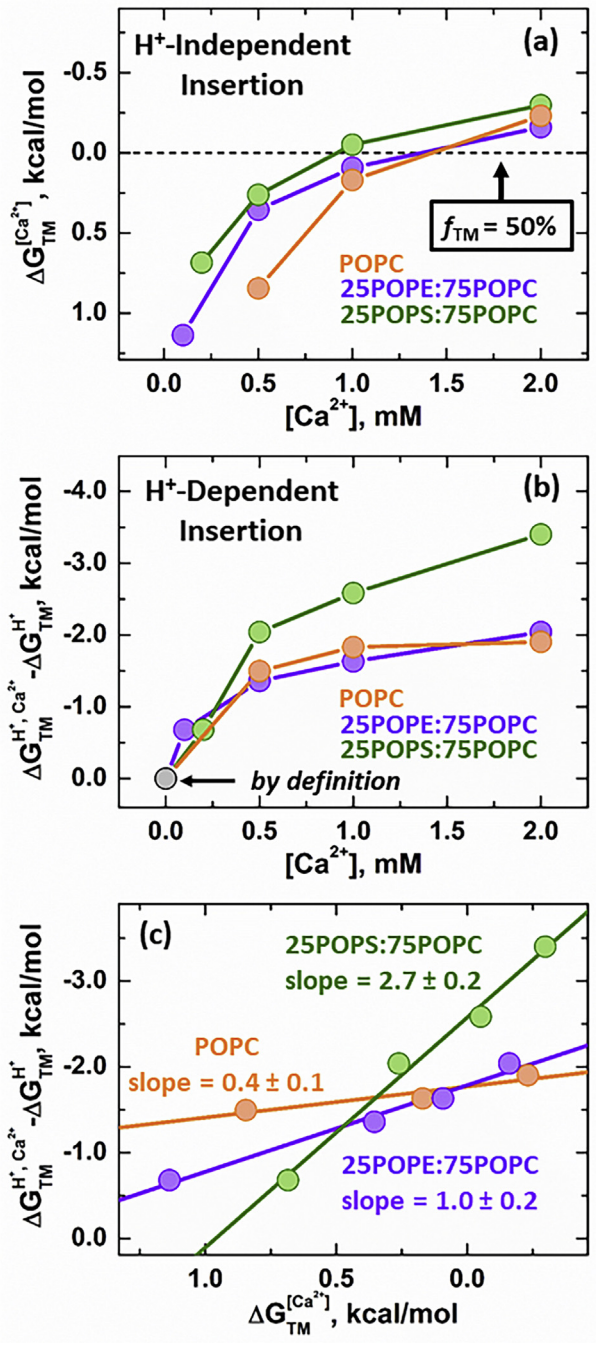

Fig. 5. Effects of Ca^2 on thermodynamics of membrane insertion of pH-Low Insertion Peptide (pHLIP). The membrane insertion of pHLIP into POPC (orange), 25POPE:75POPC (purple), and 25POPS:75POPC (green) large unilamellar vesicles (LUV) was measured as a function of pH at [Ca^{2+}] ranging from 0 to 2.0 mM (for complete set of raw data see Fig. S4). (a) The effect of Ca^{2+} on the free energy of pH-independent insertion of pHLIP $\Delta G_{TM}^{[Ca2+]}$, calculated using Eq. (4). This free energy is based on the fractional insertion f_{TM} measured at pH 10.0 and equals $\Delta G_{TM}^{[Ca2+]} = 0$ kcal/mol when half of pHLIP molecules are inserted (dashed line). (b) The effect of Ca^{2+} on the free energy of protonation-dependent insertion of pHLIP, calculated from the pK_as according to Eq. (3). For each lipid composition, the data are plotted as a difference between the free energy in the presence of Ca^{2+} ($\Delta G_{TM}^{H+,\ Ca2+}$) and the corresponding free energy in the absence of Ca^{2+} (ΔG_{TM}^{H+}). By definition, all curves originate from the common origin point (*i.e.,* $\Delta G_{TM}^{H+,\ Ca2+} - \Delta G_{TM}^{H+} = 0$ kcal/mol at 0 mM Ca^{2+} for each lipid composition). (c) The cross-correlation of the free energies determined for the protonation-dependent and protonation-independent insertion of pHLIP. For each concentration of Ca^{2+}, the pH-independent mode (obtained from panel a) is plotted against the free energy difference for pH-dependent mode (obtained from panel b). The lines represent the linear approximations for each lipid composition with the following parameters: Slopes: POPC = 0.4 ± 0.1, 25POPE:75POPC = 1.0 ± 0.2, and 25POPS:75POPC = 2.7 ± 0.2. Intercepts (y value at x = 0): POPC = −1.8 kcal/mol, 25POPE:75POPC = −1.8 kcal/mol, and 25POPS:75POPC = −2.6 kcal/mol. POPC, palmitoyl-oleoyl-phosphatidylcholine; POPE, 1-palmitoyol-2-oleoyl-*sn-glycero-3-phosphoethanolamine; POPS, palmitoyl-oleoyl-phosphatidylserine.*

25POPE:75POPC LUV showed a reduced effect for Mg^{2+} compared with Ca^{2+}, resulting in a 9 nm blue shift to 347 nm from 356 nm (Fig. S5c), compared to the 12 nm blue shift in the presence of Ca^{2+} (Fig. 4c). Measurements with 25POPS:75POPC also showed a reduced effect when compared with Ca^{2+}. In the case of these anionic bilayers, the presence of Mg^{2+} only resulted in a 4 nm maximal blue shift to 352 nm from 356 nm in the absence of divalent cations (Fig. S5e). The inability of Mg^{2+} to yield the same blue shifts as equimolar concentrations of Ca^{2+} indicates that Mg^{2+} is less efficient in promoting the transition of pHLIP into its transmembrane state. Despite these weaker effects, the ability of Mg^{2+} to induce the transmembrane insertion of pHLIP without lowering the pH was confirmed by OCD measurements (Fig. S6). The intermediate Trp fluorescence maxima were therefore interpreted as a combination of transmembrane and interfacial pHLIP populations.

We also performed pH-titrations in the presence of 2.0 mM Mg^{2+} and vesicles with different composition (POPC, 25POPE:75POPC, and 25POPS:75POPC). As in the case of Ca^{2+}, the presence of Mg^{2+} led to a decrease in the Trp fluorescence maximum at pH 10.0 compared with measurements in the absence of divalent cations (Figs. S5b, d, and f). This is consistent with the Mg^{2+}-dependent insertion of pHLIP into membranes without the need for protonation. This effect appears to be more moderate with Mg^{2+} than with Ca^{2+} (Fig. 4b, d, and f). The decrease in Trp position of maximum at pH 10.0 was accompanied by a shift of the curves toward alkali pH (Fig. S5, blue arrows). The

magnitude of this shift, however, was reduced compared with equimolar concentrations of Ca^{2+}. In the case of POPC, the presence of 2.0 mM Mg^{2+} led to a 1.0 pH unit increase in its pK_a from 6.1 ± 0.1 to 7.1 ± 0.1 (Fig. S5b), compared with the 1.5 pH units gain in the case of Ca^{2+} (Fig. 4b). Similarly, the presence of 2.0 mM Mg^{2+} increased the pK_a of the pH-dependent insertion of pHLIP into 25POPE:75-POPC LUV by 0.3 pH unit shift from 5.7 ± 0.1 to 6.1 ± 0.1 (Fig. S5d), compared with 1.5 pH unit in the presence of Ca^{2+} (Fig. 4d). A shift of the pH-titration curve toward a more basic pH range was also observed for 25POPS:75POPC bilayers when 2.0 mM Mg^{2+} was present (Fig. S6f). The shorter buffering range of HEPES buffer compared with the traditional phosphate buffer (see Methods for details), however, limited our measurements to pH $\geq$ 6.0. This prevented us from accurately determining the pK_a under these conditions, but it was estimated to be $\leq$ 6.0 compared to 5.4 in the absence of Mg^{2+}.

Our measurements with Mg^{2+} show that the modulation of pHLIP membrane insertion is not specific to Ca^{2+}, suggesting a more general role of divalent cations in this process. Nevertheless, in all lipid compositions, the addition of Ca^{2+} had a more prominent effect compared with that of Mg^{2+}. Preferential effects of specific divalent cations, particularly for calcium, on protein membrane interactions have been previously observed for other systems such as α-synuclein [36], highlighting the importance of proper cation conditions when characterizing membrane active proteins.

Discussion

The results presented here provide new insights into our understanding of the physicochemical mechanisms underlying the ability of pHLIP to target tumors and other disease tissues. The standard pH-dependent targeting mechanism involves protonation of key acidic residues (e.g., D14 and D25) [21,33,37] and subsequent membrane insertion. At mildly acidic pH (pH < 6.0) pHLIP adopts a transmembrane conformation with characteristic spectroscopic signatures that have been well-established for model membrane systems [10,24,26]. Here, we demonstrated that addition of either Ca^{2+} or Mg^{2+}, at neutral or even basic pH, results in the same fluorescence and CD changes as those usually observed at low pH (Fig. 3). The addition of divalent cations produces two independent effects: (1) pH-independent insertion at neutral and basic pH (arrows 1 in Fig. 4b, d and f and Fig. S5b, d, and f) and (2) modulation of pK_a for the acid-driven insertion (arrows 2 in Fig. 4b, d, f and Fig. S5b, d, and f). Both effects have been found to be modulated by the lipid composition (Figs. 4 and 5), which might be a contributing factor in tumor targeting [28–32].

We illustrate the effects of divalent cations on the bilayer insertion of pHLIP using the schemes in Fig. 6a.

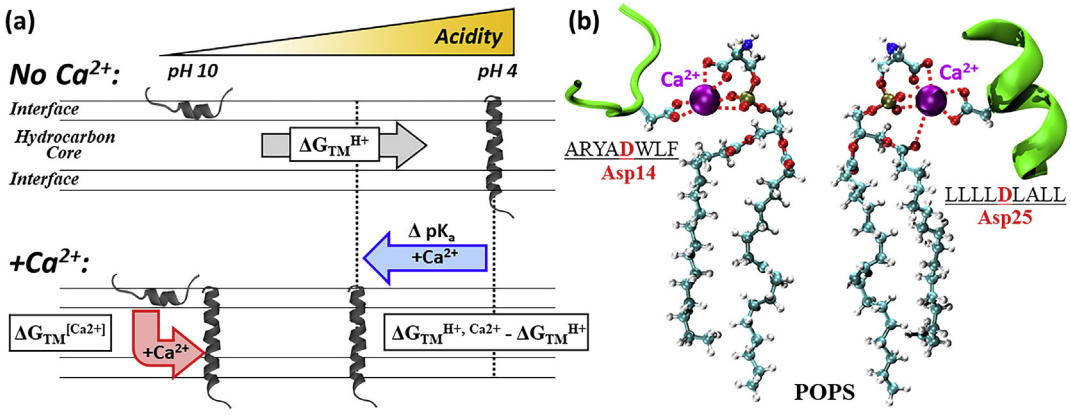

Fig. 6. Thermodynamic scheme of pH-Low Insertion Peptide (pHLIP) membrane interactions. (a) Thermodynamic scheme of pHLIP membrane insertion in the presence and absence of Ca^{2+}. In the absence of divalent cations, the only factor driving the membrane insertion of pHLIP is its protonation-dependent insertion with a ΔG_{TM}^{H+}. The presence of Ca^{2+} leads to a more favorable protonation-dependent insertion (lower acidity levels required for insertion) with a free energy of $\Delta G_{TM}^{H+, Ca2+} - \Delta G_{TM}^{H+}$. Additionally, Ca^{2+} introduces a new pH-independent membrane insertion free energy with a $\Delta G_{TM}^{[Ca2+]}$. While the scheme only shows the free energies in the presence of Ca^{2+}, other divalent cations (e.g., Mg^{2+}) with corresponding free energies are also expected to modulate pHLIP insertion (see Supplementary Fig. S5). (b) Schematic representation of pHLIP fragments in a putative unstructured and helical conformation (green) bound to POPS lipids in the presence of Ca^{2+} (purple). The coordination of Ca^{2+} by Asp 14 or Asp 25 in pHLIP and the known possible coordination sites of divalent cations [40,42,43] in POPS lipids is indicated by dashed red lines. In the case of POPC, the interactions coordinating to serine group on the lipid will be absent (e.g., top two dashed lines), resulting in weaker coupling of lipid-Ca^{2+}-protein interactions. POPS, palmitoyl-oleoyl-phosphatidylserine; POPC, palmitoyl-oleoyl-phosphatidylcholine.

The top panel contains a standard pH-dependent insertion scheme [19,20,24], which depicts the conversion of the interfacial unfolded state, populated at high and neutral pH, and the transmembrane helical state, populated al low pH. Insertion is characterized by the transition pK_a, which is influenced by both mutations of pHLIP [18–20,38] and variations in lipid composition [17,19,20,27,39]. The free energy for this protonation-dependent transition, ΔG_{TM}^{H+}, is calculated from the pK_as using Eq. (3). The presence of divalent cations investigated here requires revising this standard pH-dependent insertion scheme (Fig. 6a, lower panel). Indeed, the presence of Ca^{2+} introduces two major effects: induction of the protonation independent insertion at neutral and acidic pH (red arrow) and the modulation of the acid-induced insertion (blue arrow). The first transition is characterized by a free energy $\Delta G_{TM}^{[Ca2+]}$, calculated using Eq. (4); and the results are presented in Fig. 5a. The second transition is best described by the difference in free energies of protonation in the presence and absence of Ca^{2+} $\Delta G_{TM}^{H+,\ Ca2+}$ - ΔG_{TM}^{H+}, calculated separately for each lipid composition (Fig. 5b). The cross-correlation analysis of the free energies of pH-dependent and pH-independent effects of Ca^{2+} is shown in Fig. 5c and discussed below.

The interplay between lipid composition and calcium concentrations on pHLIP membrane insertion is best illustrated by the plots of the corresponding free energies for pH-dependent and calcium-induced insertion (Fig. 5c). For pure POPC, the dependence is rather shallow, suggesting a limited ability of pH-dependent modulation by Ca^{2+} on the insertion of pHLIP. For a 25POPE:75POPC lipid composition, the slope equals one, suggesting that both effects are equally important. The presence of 25% POPS results in a dramatic increase of the slope, indicating that POPS when coupled with Ca^{2+} strongly promotes pH-dependent insertion. We speculate that the reasons for this lipid-dependent modulation of insertion thermodynamics may be related to the ability of different lipids to co-coordinate divalent cations with the acidic side chains of pHLIP (Fig. 6b).

It has been long established that interactions of cations with lipid bilayers depend on the nature of the cation and the lipid headgroups [39]. However, the complex nature of these interactions is still an active area of experimental and computational research. For example, Melcrova and coauthors recently demonstrated that lipid membranes have substantial calcium-binding capacity, with several types of binding sites present [40]. It is worth noting that the mechanism of action of Ca^{2+} and Mg^{2+} on the insertion of pHLIP is not likely to involve changes in surface potential. This is evident from the fact that the effects of divalent cations led to pK_a shifts in the opposite direction as those caused by the decrease in surface potential due to the additions of high concentrations of monovalent cations [41] or the decrease of anionic lipid content [19,20].

While the exact nature of the coupling between lipid headgroups and divalent cations in the insertion of pHLIP requires further investigation, it is reasonable to assume that the ability of Ca^{2+} and Mg^{2+} to coordinate bonding with lipid headgroups and acidic residues plays an important role. This effect has been illustrated in Fig. 6b, which shows the putative interaction between POPS lipids and the unstructured and helical conformations of pHLIP (Fig. 6b, green) in the presence of Ca^{2+}. We hypothesize that divalent cations (Fig. 6, purple spheres) mediate this interaction through anionic residues in pHLIP (e.g., D14 and D25, indicated in red), which are involved in its protonation-mediated folding and insertion [9,21,33,37]. It should be noted that in the case of POPS we expect Ca^{2+} and Mg^{2+} to be coordinated not just by the phosphates present in the lipids and anionic groups in pHLIP (dashed lines), but also by the POPS anionic head group or possibly its ester oxygens [40,42,43]. Zwitterionic lipids on the other hand lack a coordination group in their head group, which would lead to lower binding of divalent cations and a lessening of the Ca^{2+}/Mg^{2+}-mediated effects on pHLIP insertion. Similar interactions have been suggested for other membrane-binding proteins in the literature [36,44–46].

How does this new knowledge on the role of Ca^{2+} and Mg^{2+} change our understanding of the mechanism of selective targeting of tumor cells by pHLIP? The conventional explanation relies on the mild acidification produced by tumors, which lowers the outside pH to ~7.0, supposedly providing the necessary selectivity [15]. While plausible for zwitterionic lipids, this explanation does not hold in the presence of anionic POPS. As demonstrated in Fig. 4f (black) and in our previous publications [19,20], no pHLIP insertion into 25POPS:75POPC bilayer is observed at pH > 5.8. As the transfer of phosphatidylserine to the outer leaflet of the plasma membrane is known to occur in cancerous cells, other mechanisms besides acidification are expected to contribute to targeting selectivity. Here, we demonstrate that divalent cations constitute an important factor, modulating interactions of pHLIP with model membranes and cells alike.

The presence of physiological concentrations of Ca^{2+} improves both cellular labeling (Fig. 1) and drug delivery by pHLIP (Fig. 2). This has important implications for the optimization of cancer imaging and targeted drug delivery strategies that rely on pHLIP variants and similar membrane-active peptides. Future strategies should account for both pH-dependent and divalent cation-dependent mechanisms as well as lipid variations in targeted cells. Moreover, the modulation of the protonation-dependent insertion pathways with Ca^{2+} and Mg^{2+} may be important for conformational switching in other

physiological processes (e.g., entry of bacterial toxins [47,48] and insertion of apoptotic regulators [49,50]).

Materials and methods

pHLIP solid-phase synthesis

pHLIP with a cysteine residue at its N-terminus (H_2N-GCEQNPIYWARYADWLF-TTPLLLLDLALLVDADEGTG-$CONH_2$) or its C-terminus (H^2N-GGEQNPIYWAR-YADWLF-TTPLLLLDLALLVDADEGTCG-$CONH_2$) were prepared by Fmoc solid-phase synthesis on an automated microwave peptide synthesizer (CEM Liberty Blue) using rink amide resin (CEM, 0.19 mmol/g loading capacity). The peptides were purified via reversed phase high-performance liquid chromatography (RP-HPLC) (Phenomenex Luna prep 5 μm Omega Polar C18 250 × 21.20 mm; flow rate 5 mL/min; phase A: water 0.1% TFA; phase B: acetonitrile 0.1% TFA; gradient 60 min from 95/5 A/B to 0/100 A/B. The purity of the peptides was determined by RP-HPLC (Phenomenex Luna 5 μm Omega Polar C18 250 × 100 mm; flow rate 5 mL/min; phase A: water 0.01% TFA; phase B: acetonitrile 0.01% TFA; gradient 60 min from 95/5 A/B to 0/100 A/B), and their identity was confirmed via MALDI-TOF MS (Shimadzu 8020).

Preparation of conjugates

Conjugating Alexa488 C5 maleimide (Invitrogen #A10254) to the N-terminus cysteine of pHLIP was achieved by dissolving pHLIP in DMF with 50 mM HEPES, pH 7.2, followed by the addition of 1 molar equivalent of Alexa488 C5 maleimide. The solution was flushed with nitrogen and mixed at room temperature for 4 h. pHLIP-MMAF was prepared by conjugating Py-ds-Prp-MMAF (Levena Biopharma) to pHLIP with a C-terminus cysteine residue utilizing the same procedure. The desired pHLIP conjugates were isolated using the same techniques described for the pHLIP peptides. The purity of the pHLIP conjugates were determined by RP-HPLC, and their identity was confirmed by MALDI-TOF MS. Alexa488-pHLIP: purity >99%; calculated $(M + H+) = 4874$, found $(M + H+) = 4874$. pHLIP-MMAF: purity >98%; calculated $(M + H+) = 5030$, found $(M + H+) = 5030$. The Alexa488-pHLIP conjugate was quantified at 493 nm by UV/Vis absorbance spectroscopy using the molar absorption coefficient of Alexa488 C5 maleimide (72,000 M^{-1} cm^{-1}). The pHLIP-MMAF conjugate was quantified at 280 nm using the molar absorption coefficient of pHLIP (13940 M^{-1} cm^{-1}). The conjugates were then lyophilized in 10^{-8} mol aliquots.

Cell culture

Human cervical adenocarcinoma HeLa and human breast adenocarcinoma MDA-MB-231 cells were cultured in Dulbecco's modified Eagle medium (DMEM) high glucose supplemented with 10% fetal bovine serum (FBS), 100 units/mL penicillin, and 0.1 mg/mL of streptomycin. The cells were cultured in a humidified atmosphere of 5% CO2 at 37 °C.

Cell viability assay

HeLa cells were plated in 96-well plates at a cell density of 5000 cells/well and incubated overnight. pHLIP-MMAF was solubilized in an appropriate volume of Dulbecco's phosphate buffered saline (DPBS) containing 1.2 mM calcium (Sigma #D8662) or lacking calcium (Sigma #D8537) pH 7.4, so that on pH adjustment, the desired treatment concentration (10 μM) was obtained. The samples were then gently sonicated for 30−60 s using a bath sonicator (Branson Ultrasonics). After removal of cell media, the cells were washed twice with phosphate-buffered saline (PBS), and then pHLIP-MMAF was added to the appropriate wells and incubated for 5 min at 37 °C. Then, the media was adjusted to the desired pH (final volume = 50 μL) using a preestablished volume of DPBS buffered with acetic acid, pH 4.0, and incubated for 2 h. Acetic acid was used for sample acidification owing to the high affinity and/or chelating properties of other acids (i.e. citric acid) toward Ca^{2+}. Following the treatment, the plate was washed once with 100 μL of complete DMEM and then recovered for 72 h at 37 °C in 100 μL of complete DMEM. Cell viability was assessed with the MTT colorimetric assay. Briefly, MTT was solubilized in PBS (10 mg/mL) with brief sonication, and 10 μL was added to each well. After incubation for 2 h at 37 °C, the formazan crystals were solubilized in 200 μL of dimethyl sulfoxide (DMSO), and the absorbance at 580 nm was measured using an Infinite F200 PRO microplate reader (Tecan). Cell viability was normalized to control cells treated with media at pH 7.4.

Cell binding experiments

MDA-MB-231 human breast cancer cells were harvested and washed twice with PBS, pH 7.4. Alexa488-pHLIP was solubilized in an appropriate volume of 10 mM HEPES, 19.5 mM NaCl, pH 7.4 without calcium so that upon a 2-fold dilution, and after pH adjustment the desired treatment concentration (1 μM) was obtained. Next, 220,000 cells were incubated in suspension with Alexa488-pHLIP at two times the desired concentration without calcium for 5 min at 37 °C. After the incubation, an equal volume of 10 mM HEPES, 19.5 mM NaCl, pH 7.4 containing either 0, 2.4, or 3.6 mM calcium was added to bring the final calcium concentration to 0, 1.2, 1.8 mM, and incubated for an additional 5 min at 37 °C. Then, the pH was adjusted (final volume = 300 μL) using a preestablished volume of 10 mM HEPES, 19.5 mM NaCl, containing the appropriate calcium concentration, buffered with acetic acid, pH 4.0, and incubated for 10 min at 37 °C. The cells were then washed at the same pH and calcium concentration as the treatment, and fixed with 4% paraformaldehyde (PFA) for 10 min at 4 °C. The cells were then resuspended in PBS and analyzed by flow cytometry using a BDFacs Canto II flow cytometer equipped with a 488 nm argon laser and a 530/30 bandpass filter. The data were analyzed using FACSDiva version 6.1.1 software. The fluorescence data are expressed as mean arbitrary fluorescence units and were gated to include all healthy mammalian cells. Fluorescence was normalized to cells treated at pH 7.4 with 0 mM calcium.

For microscopy, MDA-MB-231 cells were seeded on glass coverslips pretreated with polylysine and allowed to reach ~70% confluency. The cells were then treated with

Alexa488-pHLIP (1 μM) at pH 7.4 or 6.0 for 10 min at 37 °C as described above. Following the treatment, the cells were washed once at the same pH and calcium concentration as the treatment, and immediately fixed with ice cold methanol for 10 min. The fixed cells were then washed twice with PBS and incubated with 1 μg/mL Hoechst (Invitrogen #H3570) in PBS for 10 min at room temperature and washed twice again. The coverslips were mounted onto a slide with fluoromount (SouthernBiotech #0100-01) and stored at 4 °C until images were taken with a Nikon Eclipse Ti microscope with a 20× objective.

Vesicle preparation

The appropriate volume of lipid stocks dissolved in chloroform were dried under a nitrogen stream and dried overnight using high vacuum. The dried lipids were resuspended in 50 mM phosphate buffer, pH 8.0 to a final concentration of 20 mM and large unilamellar vesicles (LUV) were formed by extrusion using a Mini-Extruder (Avanti Polar Lipids, Alabaster, AL). Extrusion was performed using 0.1 μm nucleopore polycarbonate membranes (Whatman, Philadelphia, PA) and the prepared stocks were stored at −4 °C. Lipids used in this study: Palmitoyl-oleoyl-phosphatidylcholine (POPC), palmitoyl-oleoyl-phosphatidylserine (POPS), and 1-palmitoyol-2-oleoyl-sn-glycero-3-phosphoethanolamine (POPE) were purchased from Avanti Polar Lipids (Alabaster, AL).

Trp fluorescence measurements

The steady-state Trp fluorescence emission measurements of pHLIP were performed on a SPEX Fluorolog FL3-22 steady-state fluorescence spectrometer (Jobin Yvon, Edison, NJ) equipped with double-grating excitation and emission monochromators. Experiments were carried out on 2 × 10 mm cuvettes oriented perpendicular to the excitation beam. Sample temperature was maintained constant at 25 °C using a Peltier device from Quantum Northwest (Spokane, WA.). Measurements were performed using 2 μM pHLIP and 1.0 mM LUV after 20 min sample equilibration. Spectra were collected between 300 and 450 nm with an excitation wavelength of 285 nm at 1.0 nm steps, using 3.0 and 4.0 nm slits on the excitation and emission monochromators, respectively, and averaged over 3 scans. The positions of maximum of the averaged spectra were determined by fitting them to a log-normal distribution using the following formula [51]:

$$For\ \lambda > \lambda_{max} - \frac{\rho\Gamma}{\rho^2 - 1},$$

$$I(\lambda) = I_0 exp\left[\frac{ln2}{ln^2\rho} ln^2\left(1 + \frac{(\lambda - \lambda_{max})(\rho^2 - 1)}{\rho\Gamma}\right)\right] \quad (1a)$$

$$While\ for\ \lambda < \lambda_{max} - \frac{\rho\Gamma}{\rho^2 - 1}, I(\lambda) = 0 \quad (1b)$$

where I_0 is the maximal intensity of the analyzed spectrum at the fluorescence maximum λ_{max}, Γ is the width of the spectrum at the half maximum intensity, and ρ represents the asymmetry of the distribution.

Experiments performed between pH 8.0 and 4.0 in the absence of Ca^{2+} or Mg^{2+} were carried out in 10 mM phosphate buffer. The high binding propensity of phosphates for divalent cations which then precipitate as a salt makes this buffer unsuitable for measurements in the presence of Ca^{2+} or Mg^{2+}. For this reason, we substituted 10 mM phosphate buffer for either 10 mM HEPES +19.5 mM NaCl (experiments between pH 8.0-6.0) or 10 mM borate buffer + 19.5 mM NaCl (experiments at pH > 8.0) due to their lack of affinity for Ca^{2+} or Mg^{2+}. The shorter buffering range of HEPES buffer, however, limited the experimental pH range to pH ≥ 6.0. Sample acidification was achieved by the addition of small aliquots of acetic/acetate buffer. As in the case of several buffers, many acids commonly used to induce acidification (i.e. citrate) chelate Ca^{2+} and Mg^{2+}, eliminating any divalent cation-mediated effect. Acetate, however, is compatible with assays performed in the presence of Ca^{2+} or Mg^{2+}. Divalent cation titrations were performed at pH 10.0 to minimize possible contribution form protonation events in our measurements.

The pK_a of the protonation-dependent insertion of pHLIP into LUV was calculated by fitting the data to the following equation using nonlinear least-square analysis [19,38]:(2)

$$\lambda = \frac{\lambda_N + \lambda_L\left(10^{m(pK_a - pH)}\right)}{1 + 10^{m(pK_a - pH)}} \quad (2)$$

where λ is the Trp position of maximum measured as a function of pH, the λ_N and λ_L parameters correspond to the saturating Trp positions of maximum at high and low pH, m is the slope of the transition, and pK_a denotes the negative logarithm of the dissociation constant.

Membrane insertion calculations

The protonation-dependent membrane insertion free energy (ΔG_{TM}^{H+}) was calculated using the following equation:(3)

$$\Delta G_{TM}^{H+} = -2.3RT \cdot pK_a \quad (3)$$

where R is the gas constant (1.985×10^{-3} kcal K^{-1} mol^{-1}) and T is the experimental temperature in Kelvin (298 K). The effect of Ca^{2+} on this process is given by the term $\Delta G_{TM}^{H+,\ Ca2+}$- ΔG_{TM}^{H+} which is calculated by subtracting the protonation-dependent membrane insertion free energy in the presence of Ca^{2+} ($\Delta G_{TM}^{H+,\ Ca2+}$) from the one obtained in the absence of Ca^{2+} (ΔG_{TM}^{H+}). This term is by definition equal to zero in the absence of divalent cations and is lower in more favorable interactions.

The Ca^{2+}-induced protonation-independent membrane insertion free energy ($\Delta G_{TM}^{[Ca2+]}$) was estimated using the decreases in Trp fluorescence maximum at pH 10.0 as proxies for the transmembrane populations of pHLIP at each [Ca^{2+}] using the following formula [35]:(4)

$$\Delta G_{TM}^{[Ca2+]} = -RTln\left(\frac{f_{TM}}{f_{IF}}\right) \quad (4)$$

where $\Delta G_{TM}^{[Ca2+]}$ represents the free energy of the Ca^{2+}-induced insertion of pHLIP measured at pH 10.0 for a particular [Ca^{2+}], R and T denote the gas constant (1.985 $\times$ 10^{-3} kcal K^{-1} mol^{-1}) and experimental temperature (298 K), respectively, and f_{TM} and f_{IF} correspond to the fractional transmembrane and interfacial populations. For reference, a $\Delta G_{TM}^{[Ca2+]} = 0$ kcal/mol represents a $f_{TM} = 0.5$, a $\Delta G_{TM}^{[Ca2+]} < 0$ kcal/mol represents a $f_{TM} > 0.5$, and a $\Delta G_{TM}^{[Ca2+]} > 0$ kcal/mol represents a $f_{TM} < 0.5$.

Circular dichroism and oriented circular dichroism

Circular dichroism (CD) and oriented CD (OCD) measurements were performed using an upgraded JASCO-720 spectropolarimeter (JASCO, Easton, MD). CD spectra were collected using 15.0 μM pHLIP and 1.0 mM POPC LUV on a 1.0 mm optical path cuvette and corrected to their appropriate backgrounds. At least 30 scans were collected for each spectrum and averaged for each sample. As for fluorescence, measurements in the presence of divalent cations were performed using 10 mM HEPES buffer + 19.5 NaCl, while 10 mM phosphate buffer was employed for experiments in the absence of divalent cations and acidification induced by acetic/acetate buffer.

OCD spectra were obtained by creating a stack of oriented multilayers on a quartz disc as previously described [52]. This technique allows the differentiation of interfacial α-helices, which present with a double minimum at ~205 and 222 nm, from transmembrane α-helices, which have a single minimum at ~228 nm [52,53]. Briefly, pHLIP and POPC lipids were codissolved at a 1:100 ratio in methanol (10 mM lipids and approximately 0.1 mM pHLIP) and 2.5 μL of the mixture was layered carefully on a ~1.0 cm circle at the center of a 2.5 cm disc. The solvent was then air dried and hydrated using warm air at ~100% relative humidity. The prepared disc was mounted on a sealed tube with the sample side pointing inward. Samples were kept hydrated by placing a drop of water in the tube before closing. At least 50 scans were collected at four different orientations increasing by 90°-angles along the central axis and averaged. For measurements in the presence of divalent cations a 2 μL drop of 2.0 mM Ca^{2+} or Mg^{2+} dissolved in 5.0 mM HEPES buffer was added in-between each bilayer of the multilayer stack. Similarly, a drop of buffer at pH 4.0 was added in-between each layer for the collected spectrum at low pH. Buffer drops were completely dried before continuing with the multilayer stack protocol. The background signal was determined by collecting the spectra of a multilayer stack in the absence of pHLIP. The data are presented normalized to the ellipticity of their minima due to difficulties calculating the peptide concentration present.

LUV aggregation measurements

The aggregation of LUV containing POPC, 25POPS:75POPC, 25POPE:75POPC, and 75POPS:25POPC (as a control) in the presence of increasing concentrations of Ca^{2+} or Mg^{2+} were determined by measuring light scattering changes at 400 nm as previously described [54,55]. Samples were performed on a 4 $\times$ 10 mm quartz cuvette containing 0.1% LUV in 10 mM HEPES buffer + 19.5 mM NaCl. Cuvette orientation did not affect the results obtained. Similar measurements have been previously performed to characterize the aggregation of 100 POPS vesicles and shown to reproduce results obtained by small-angle scattering and dynamic light scattering [54,55].

Acknowledgments

This work was supported by National Institutes of Health (R01 GM126778 to A.S.L. and R21CA181868 to D.T.) and by Lehigh University to D.T. We are very grateful to Dr. William Wimley (Tulane University) for lending us his OCD holder and to Dr. Alexander Kyrychenko (Karazin University) for making an illustration in Fig. 6b.

Contributions

V.V.M. designed and carried out biophysical experiments; analyzed the data; wrote the manuscript. J.G. synthesized and labeled peptides and carried out and analyzed cellular experiments. D.T. designed and interpreted cellular experiments; wrote the manuscript. A.S.L. designed and interpreted experiments and wrote the manuscript.

Appendix A. Supplementary data

Supplementary data to this article can be found online at https://doi.org/10.1016/j.jmb.2019.10.016.

Received 21 July 2019;
Received in revised form 24 October 2019;
Accepted 24 October 2019
Available online 2 November 2019

Keywords:
pH-dependent membrane insertion;
Tryptophan fluorescence;
Membrane-associated folding;
Tumor targeting;
Drug delivery

References

[1] O.A. Andreev, D.M. Engelman, Y.K. Reshetnyak, Targeting diseased tissues by pHLIP insertion at low cell surface pH, Front. Physiol. 5 (2014) 97, https://doi.org/10.3389/fphys.2014.00097.

[2] Y.K. Reshetnyak, et al., Measuring tumor aggressiveness and targeting metastatic lesions with fluorescent pHLIP, Mol. Imaging Biol. 13 (2010) 1146–1156.
[3] O.A. Andreev, D.M. Engelman, Y.K. Reshetnyak, pH-sensitive membrane peptides (pHLIPs) as a novel class of delivery agents, Mol. Membr. Biol. 27 (2010) 341–352.
[4] L.C. Wyatt, J.S. Lewis, O.A. Andreev, Y.K. Reshetnyak, D.M. Engelman, Applications of pHLIP technology for cancer imaging and therapy: (trends in biotechnology 35, 653-664, 2017), Trends Biotechnol. 36 (1300) (2018), https://doi.org/10.1016/j.tibtech.2017.11.005.
[5] C.J. Cheng, et al., MicroRNA silencing for cancer therapy targeted to the tumour microenvironment, Nature 518 (2015) 107–110, https://doi.org/10.1038/nature13905.
[6] Y.K. Reshetnyak, O.A. Andreev, U. Lehnert, D.M. Engelman, Translocation of molecules into cells by pH-dependent insertion of a transmembrane helix, Proc. Natl. Acad. Sci. U.S.A. 103 (2006) 6460–6465.
[7] D. Thevenin, M. An, D.M. Engelman, pHLIP-mediated translocation of membrane-impermeable molecules into cells, Chem. Biol. 16 (2009) 754–762, https://doi.org/10.1016/j.chembiol.2009.06.006.
[8] A.G. Karabadzhak, et al., pHLIP-FIRE, a cell insertion-triggered fluorescent probe for imaging tumors demonstrates targeted cargo delivery in vivo, ACS Chem. Biol. 9 (2014) 2545–2553, https://doi.org/10.1021/cb500388m.
[9] S.A. Otieno, et al., pH-dependent thermodynamic intermediates of pHLIP membrane insertion determined by solid-state NMR spectroscopy, Proc. Natl. Acad. Sci. U.S.A. 115 (2018) 12194–12199, https://doi.org/10.1073/pnas.1809190115.
[10] J.F. Hunt, P. Rath, K.J. Rothschild, D.M. Engelman, Spontaneous, pH-dependent membrane insertion of a transbilayer α-helix, Biochemistry 36 (1997) 15177–15192.
[11] A.I. Hashim, X. Zhang, J.W. Wojtkowiak, G.V. Martinez, R.J. Gillies, Imaging pH and metastasis, NMR Biomed. 24 (2011) 582–591, https://doi.org/10.1002/nbm.1644.
[12] M. Damaghi, J.W. Wojtkowiak, R.J. Gillies, pH sensing and regulation in cancer, Front. Physiol. 4 (2013) 370, https://doi.org/10.3389/fphys.2013.00370.
[13] V.P. Nguyen, D.S. Alves, H.L. Scott, F.L. Davis, F.N. Barrera, A novel soluble peptide with pH-responsive membrane insertion, Biochemistry 54 (2015) 6567–6575, https://doi.org/10.1021/acs.biochem.5b00856.
[14] D.S. Alves, et al., A novel pH-dependent membrane peptide that binds to EphA2 and inhibits cell migration, eLife 7 (2018), https://doi.org/10.7554/eLife.36645.
[15] M. An, D. Wijesinghe, O.A. Andreev, Y.K. Reshetnyak, D.M. Engelman, pH-(low)-insertion-peptide (pHLIP) translocation of membrane impermeable phalloidin toxin inhibits cancer cell proliferation, Proc. Natl. Acad. Sci. U.S.A. 107 (2010) 20246–20250.
[16] G.B. Ding, et al., Robust anticancer efficacy of a biologically synthesized tumor acidity-responsive and autophagy-inducing functional beclin 1, ACS Appl. Mater. Interfaces 10 (2018) 5227–5239, https://doi.org/10.1021/acsami.7b17454.
[17] H.L. Scott, F.A. Heberle, J. Katsaras, F.N. Barrera, Phosphatidylserine asymmetry promotes the membrane insertion of a transmembrane helix, Biophys. J. 116 (2019) 1495–1506, https://doi.org/10.1016/j.bpj.2019.03.003.
[18] D. Weerakkody, et al., Family of pH (low) insertion peptides for tumor targeting, Proc. Natl. Acad. Sci. U.S.A. 110 (2013) 5834–5839, https://doi.org/10.1073/pnas.1303708110.
[19] A. Kyrychenko, V. Vasquez-Montes, M.B. Ulmschneider, A.S. Ladokhin, Lipid headgroups modulate membrane insertion of pHLIP peptide, Biophys. J. 108 (2015) 791–794, https://doi.org/10.1016/j.bpj.2015.01.002.
[20] V. Vasquez-Montes, J. Gerhart, K.E. King, D. Thevenin, A.S. Ladokhin, Comparison of lipid-dependent bilayer insertion of pHLIP and its P20G variant, Biochim. Biophys. Acta Biomembr. 1860 (2018) 534–543, https://doi.org/10.1016/j.bbamem.2017.11.006.
[21] M. Musial-Siwek, A. Karabadzhak, O.A. Andreev, Y.K. Reshetnyak, D.M. Engelman, Tuning the insertion properties of pHLIP, Biochim. Biophys. Acta 1798 (2010) 1041–1046.
[22] K.E. Burns, H. Hensley, M.K. Robinson, D. Thevenin, Therapeutic efficacy of a family of pHLIP-MMAF conjugates in cancer cells and mouse models, Mol. Pharm. 14 (2017) 415–422, https://doi.org/10.1021/acs.molpharmaceut.6b00847.
[23] K.E. Burns, M.K. Robinson, D. Thevenin, Inhibition of cancer cell proliferation and breast tumor targeting of pHLIP-monomethyl auristatin E conjugates, Mol. Pharm. 12 (2015) 1250–1258, https://doi.org/10.1021/mp500779k.
[24] Y.K. Reshetnyak, M. Segala, O.A. Andreev, D.M. Engelman, A monomeric membrane peptide that lives in three worlds: in solution, attached to, and inserted across lipid bilayers, Biophys. J. 93 (2007) 2363–2372.
[25] Y. Wu, H.W. Huang, G.A. Olah, Method of oriented circular dichroism, Biophys. J. 57 (1990) 797–806, https://doi.org/10.1016/S0006-3495(90)82599-6.
[26] O.A. Andreev, et al., pH (low) insertion peptide (pHLIP) inserts across a lipid bilayer as a helix and exits by a different path, Proc. Natl. Acad. Sci. U.S.A. 107 (2010) 4081–4086, https://doi.org/10.1073/pnas.0914330107.
[27] A.G. Karabadzhak, et al., Bilayer thickness and curvature influence binding and insertion of a pHLIP peptide, Biophys. J. 114 (2018) 2107–2115, https://doi.org/10.1016/j.bpj.2018.03.036.
[28] T. Utsugi, A.J. Schroit, J. Connor, C.D. Bucana, I.J. Fidler, Elevated expression of phosphatidylserine in the outer membrane leaflet of human tumor cells and recognition by activated human blood monocytes, Cancer Res. 51 (1991) 3062–3066.
[29] S. Riedl, et al., In search of a novel target - phosphatidylserine exposed by non-apoptotic tumor cells and metastases of malignancies with poor treatment efficacy, Biochim. Biophys. Acta 2011 (1808) 2638–2645, https://doi.org/10.1016/j.bbamem.2011.07.026.
[30] R.F. Zwaal, P. Comfurius, E.M. Bevers, Surface exposure of phosphatidylserine in pathological cells, Cell. Mol. Life Sci. : CMLS 62 (2005) 971–988, https://doi.org/10.1007/s00018-005-4527-3.
[31] L.T. Tan, et al., Targeting membrane lipid a potential cancer cure? Front. Pharmacol. 8 (2017) 12, https://doi.org/10.3389/fphar.2017.00012.
[32] J.H. Stafford, P.E. Thorpe, Increased exposure of phosphatidylethanolamine on the surface of tumor vascular endothelium, Neoplasia 13 (2011) 299–308, https://doi.org/10.1593/neo.101366.
[33] J. Fendos, F.N. Barrera, D.M. Engelman, Aspartate embedding depth affects pHLIP's insertion pK, Biochemistry (2013), https://doi.org/10.1021/bi400252k.
[34] T. Hessa, et al., Recognition of transmembrane helices by the endoplasmic reticulum translocon, Nature 433 (2005) 377–381.

[35] M.B. Ulmschneider, J.C. Smith, J.P. Ulmschneider, Peptide partitioning properties from direct insertion studies, Biophys. J. 98 (2010) L60–L62, https://doi.org/10.1016/j.bpj.20103.043.
[36] J. Lautenschlager, et al., C-terminal calcium binding of alpha-synuclein modulates synaptic vesicle interaction, Nat. Commun. 9 (2018) 712, https://doi.org/10.1038/s41467-018-03111-4.
[37] O.A. Andreev, et al., Mechanism and uses of a membrane peptide that targets tumors and other acidic tissues in vivo, Proc. Natl. Acad. Sci. U.S.A. 104 (2007) 7893–7898.
[38] J. Fendos, F.N. Barrera, D.M. Engelman, Aspartate embedding depth affects pHLIP's insertion pKa, Biochemistry 52 (2013) 4595–4604, https://doi.org/10.1021/bi400252k.
[39] A. Lau, A. McLaughlin, S. McLaughlin, The adsorption of divalent cations to phosphatidylglycerol bilayer membranes, Biochim. Biophys. Acta 645 (1981) 279–292.
[40] A. Melcrova, et al., The complex nature of calcium cation interactions with phospholipid bilayers, Sci. Rep. 6 (2016) 38035, https://doi.org/10.1038/srep38035.
[41] J. Westerfield, et al., Ions modulate key interactions between pHLIP and lipid membranes, Biophys. J. 117 (2019) 920–929, https://doi.org/10.1016/j.bpj.2019.07.034.
[42] M.L. Valentine, A.E. Cardenas, R. Elber, C.R. Baiz, Physiological calcium concentrations slow dynamics at the lipid-water interface, Biophys. J. 115 (2018) 1541–1551, https://doi.org/10.1016/j.bpj.2018.08.044.
[43] P.T. Vernier, M.J. Ziegler, R. Dimova, Calcium binding and head group dipole angle in phosphatidylserine-phosphatidylcholine bilayers, Langmuir 25 (2009) 1020–1027, https://doi.org/10.1021/la8025057.
[44] H. Luecke, B.T. Chang, W.S. Mailliard, D.D. Schlaepfer, H.T. Haigler, Crystal structure of the annexin XII hexamer and implications for bilayer insertion, Nature 378 (1995) 512–515.
[45] W. Kuo, D.Z. Herrick, J.F. Ellena, D.S. Cafiso, The calcium-dependent and calcium-independent membrane binding of synaptotagmin 1: two modes of C2B binding, J. Mol. Biol. 387 (2009) 284–294, https://doi.org/10.1016/j.jmb.2009.01.064.
[46] H.O. van Genderen, H. Kenis, L. Hofstra, J. Narula, C.P. Reutelingsperger, Extracellular annexin A5: functions of phosphatidylserine-binding and two-dimensional crystallization, Biochim. Biophys. Acta 1783 (2008) 953–963, https://doi.org/10.1016/j.bbamcr.2008.01.030.
[47] R.J. Collier, J.A. Young, Anthrax toxin, Annu. Rev. Cell Dev. Biol. 19 (2003) 45–70.
[48] A.S. Ladokhin, pH-triggered conformational switching along the membrane insertion pathway of the diphtheria toxin T-domain, Toxins 5 (2013) 1362–1380, https://doi.org/10.3390/toxins5081362.
[49] A.J. Minn, et al., Bcl-x(L) forms an ion channel in synthetic lipid membranes, Nature 385 (1997) 353–357.
[50] V. Vasquez-Montes, et al., Lipid-modulation of membrane insertion and refolding of the apoptotic inhibitor Bcl-xL, Biochim. Biophys. Acta Protein Proteonomics 1867 (2019) 691–700, https://doi.org/10.1016/j.bbapap.2019.04.006.
[51] A.S. Ladokhin, S. Jayasinghe, S.H. White, How to measure and analyze tryptophan fluorescence in membranes properly, and why bother? Anal. Biochem. 285 (2000) 235–245.
[52] W.C. Wimley, S.H. White, Designing transmembrane alpha-helices that insert spontaneously, Biochemistry 39 (2000) 4432–4442.
[53] A.S. Ladokhin, S.H. White, Detergent-like' permeabilization of anionic lipid vesicles by melittin, Biochim. Biophys. Acta 1514 (2001) 253–260.
[54] A. Martin-Molina, C. Rodriguez-Beas, J. Faraudo, Effect of calcium and magnesium on phosphatidylserine membranes: experiments and all-atomic simulations, Biophys. J. 102 (2012) 2095–2103, https://doi.org/10.1016/j.bpj.20123.009.
[55] S. Ohki, A mechanism of divalent ion-induced phosphatidylserine membrane fusion, Biochim. Biophys. Acta 689 (1982) 1–11.